Effect of corrosion damage on the fatigue behavior of S460NL High-Strength Steel under cyclic loading

Mohammad Al Khazali
Brno University of Technology, Faculty of Civil Engineering, Institute of Structural Mechanics, Veveří 331/95, 602 00 Brno, Czech Republic
Mohammad.Sami.Al.Khazali@vutbr.cz, https://orcid.org/0009-0004-6998-9264

Stanislav Seitl, Lucie Malikova
Brno University of Technology, Faculty of Civil Engineering, Institute of Structural Mechanics Veveří 331/95, 602 00 Brno, Czech Republic and Czech Academy of Sciences, Institute of Physics of Materials, v. v. i., Žižkova 22, 616 00 Brno, Czech Republic
Stanislav.Seitl@vut.cz, http://orcid.org/0000-0002-4953-4324
Lucie.Malikova@vut.cz, http://orcid.org/0000-0001-5868-5717

Vít Křivý, Miroslav Vacek
VŠB-TU Ostrava, Faculty of Civil Engineering, Ludvíka Podéště 1875, 708 33 Ostrava, Czech Republic
vit.krivy@vsb.cz, https://orcid.org/0000-0002-7251-2473
miroslav.vacek@vsb.cz, https://orcid.org/0000-0002-9197-856X

ABSTRACT. The present study investigates the influence of corrosion exposure on the fatigue behavior of S460NL high-strength structural steel, a material that is frequently utilized in offshore and civil engineering structures. Accelerated corrosion was simulated under controlled laboratory conditions for exposure periods of 3 days, 6 days, and 6 + 3 days, in addition to specimens subjected to natural atmospheric corrosion. To this end, fatigue tests were performed to obtain *S–N* curves, and the results were evaluated using Basquin's law and the probabilistic Castillo–Canteli model.

The findings indicate that corrosion has a substantial impact on fatigue resistance. The endurance limit exhibited a decline from 214 MPa for the reference specimens to 176 MPa following three days of corrosion, 135 MPa after six days, and approximately 92 MPa after combined corrosion exposure, signifying a reduction of up to 57%. Fractographic observations revealed that corrosion pits act as stress concentrators, thereby promoting early crack

Citation: Al Khazali, M.S., Seitl, S., Malíkova, L., Křivý, V., Vacek, M., Effect of Corrosion Damage on the Fatigue Behavior of S460NL High-Strength Steel under Cyclic Loading, Fracture and Structural Integrity, 77 (2026) 56-77.

Received: 04.02.2026
Accepted: 30.03.2026
Published: 04.04.2026
Issue: 07.2026

initiation. A discernible correlation was identified between corrosion mass loss and normalized endurance limit.
These findings highlight the importance of considering corrosion effects in fatigue life assessment and structural design of high-strength steel components.

KEYWORDS. S460NL, Fatigue, Corrosion, S-N curve, Canteli model, Basquin law.

INTRODUCTION

High-strength steels (HSS) have seen a substantial increase in utilization within the domain of civil engineering structures. This is primarily attributed to the advantageous strength-to-weight ratio exhibited by these materials, as well as the potential to engineer more lightweight and efficient structural components. The structural application of these elements is supported by the provisions of Eurocode 3 (EN 1993-1-1 and EN 1993-1-12) [1,2]. Steels of strength class S460 have been successfully applied in major bridge structures, such as the Øresund Bridge and the Millau Viaduct [3,4], and their use in conventional steel–concrete composite bridges has also increased in recent years[5].
Despite these advantages, the long-term durability of structures made from HSS is strongly influenced by fatigue loading and corrosion processes, which often act simultaneously in real structures[6]. Corrosion damage frequently results in the formation of pits and surface irregularities[7–9]. These defects act as stress concentrators, thereby accelerating fatigue crack initiation[10–13]. A number of studies have previously investigated the fatigue behavior of high-strength steels and corrosion-affected structural components [6,14–16]. These studies demonstrate that corrosion significantly reduces fatigue life due to localized surface damage and stress concentration effects.
However, the quantitative relationship between corrosion severity and fatigue resistance degradation in S460NL structural steel has not been sufficiently clarified, particularly when comparing accelerated laboratory corrosion with natural atmospheric exposure conditions [17,18].
Therefore, the present study investigates the fatigue behavior of S460NL high-strength steel subjected to different corrosion exposure conditions. Accelerated corrosion tests and natural atmospheric exposure were combined with *S–N* fatigue testing. The obtained fatigue data were evaluated using Basquin's law and the probabilistic Castillo–Canteli model in order to quantify the degradation of fatigue resistance and to establish a correlation between corrosion damage and endurance limit reduction [19,20].

Chemical component	Percentage (%)
Fe	bal.
C	0.171
Si	0.472
Mn	1.680
P	0.016
S	0.001
Al	0.019
Cr	0.036
Ni	0.020
Mo	0.013
Cu	0.009
V	0.115
Nb	0.003
Ti	0.002
N	0.025
B	0.001
Cae	0.490

Table 1. Chemical composition of S460NL, according to the producer's list (Cae = C+(Mn/6)+(Cr+Mo+V)/5+(Ni+Cu)/15)

EXPERIMENTAL INVESTIGATION

Material (S460NL)

S460NL steel was used for testing. The chemical composition of HSS grades S460NL is specified in the EN-10025-6 standard [21] and presented in Tab. 1. The tensile test curves of S460NL are shown in Fig. 1. The S460NL mechanical properties with index of dispersion are given in Tab. 2.

S460NL	Average values	Average deviation
Yield strength σ_{yL} [MPa]	471	±1.6
Tensile strength σ_u [MPa]	625	±3.8
Modulus of elasticity E [GPa]	213	±9.1
Ductility A_{gt} [%]	27.46	±1.9

Table 2. Average values of S460NL mechanical properties together with average deviation

The variability of mechanical properties was quantified using the average deviation (standard deviation) obtained from multiple tensile tests.

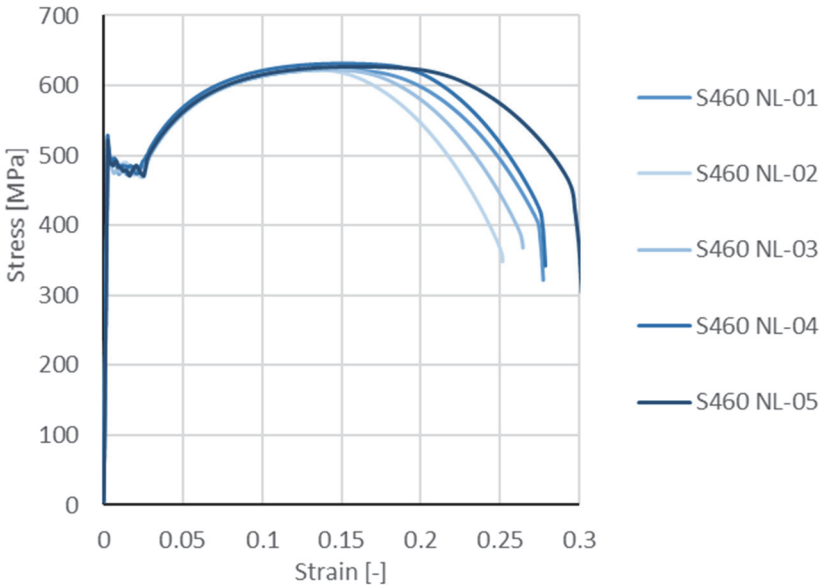

Figure 1. Monotonic stress–strain curves obtained from a tensile test for S460NL.

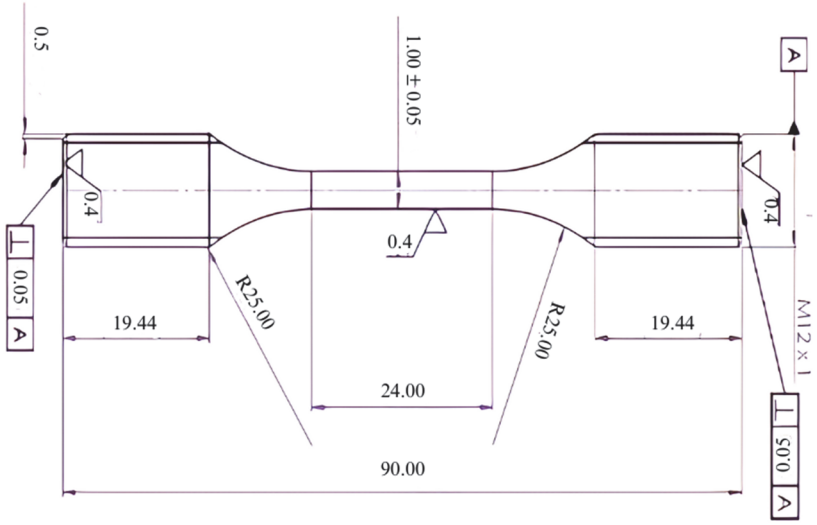

Figure 2. Shape and dimensions of steel specimens for fatigue tests.

Fatigue test specimens

Fatigue specimens were prepared in accordance with ASTM E466 [22]. For each corrosion condition, 12 specimens were prepared for each series (5×12=60 specimens were prepared for fatigue tests); the specimen shape and size is shown in Fig. 2. The specimens for fatigue testing were made from 20 mm thick S460NL steel plates perpendicular to rolling direction.

Corrosion of the specimens

Accelerated corrosion tests were performed using the Ascott S2000is corrosion chamber following the procedures outlined in the ISO 9227 salt spray test standard [23]. The specimens were subjected to two distinct chamber modes to simulate different corrosive environments.

- Mode 1: The chamber temperature was maintained at +35°C, while the humidifier temperature was set to +48°C.
- Mode 2: The chamber temperature increased to +50°C, with the humidifier temperature remaining at +48°C.

In both modes, a 5% NaCl solution was used to generate salt mist, which provided a consistent corrosive environment. The specimens were exposed to salt mist in the following conditions:

- 3 Days in Mode 1: Specimens were exposed to salt mist for 3 days at +35°C.
- 6 Days in Mode 1: Specimens were exposed to salt mist for 6 days at +35°C.
- 6 Days in Mode 1 followed by 3 Days in Mode 2: Specimens were first exposed to salt mist for 6 days at +35°C and then for an additional 3 days at +50°C.
- Additional specimens were exposed to natural atmospheric conditions on the roof of the Experimental and Diagnostic Building Center at VŠB–Technical University of Ostrava from April 2022 to October 2023. The site is characterized by an urban environment with relatively low industrial pollution and moderate traffic intensity. During the exposure period, environmental parameters such as temperature, precipitation, and relative humidity were monitored to characterize the corrosion environment. The recorded temperature ranged approximately from –5 °C in winter to 30 °C in summer, with an average relative humidity of about 70% and total precipitation of approximately 600 mm during the exposure period. The weather data can be accessed through; Meteocentrum Weather Archive.

Fig. 3 shows the specimens placed inside the corrosion chamber, while Fig. 4 presents the specimens exposed to natural atmospheric conditions.

Figure 3. S460NL fatigue specimens placed inside the Ascott S2000is corrosion chamber during the accelerated salt spray corrosion test according to ISO 9227. The specimens correspond to the corrosion exposure groups of 3 days (35°C), 6 days (35°C), and 6 days (35°C) + 3 days (50°C). Plastic covers were used to protect the threaded ends of the specimens from corrosion.

Figure 4. S460NL fatigue specimens exposed to natural atmospheric conditions on the roof of the Experimental and Diagnostic Building Center at VŠB–TU Ostrava. The specimens were mounted on an outdoor exposure frame to simulate real environmental conditions. Plastic covers were used to protect the threaded ends of the specimens from corrosion.

Typical specimens of steel S460NL for fatigue experiments without and with four various levels of corrosion are shown in Fig. 5.

Figure 5. Examples of steel specimens for fatigue experiments without and with four various levels of corrosion. Reference; 3 (35°C) days; 6 (35°C) days; 6 (35°C) +3 (50°C) days specimens and specimen from natural exposure (from left to right).

METHODS OF MEASUREMENT AND EVALUATION

Fatigue test set up

Fatigue tests were performed using a ZwickRoell Vibrophore resonance pulsator (Fig. 6). The specimens were subjected to constant-amplitude axial loading with a stress ratio of $R = 0.1$. The contractual fatigue limit was defined at $N = 10^7$ cycles, and the loading frequency varied between 70 and 110 Hz depending on the stress level. The tests were performed in laboratory air at temperature 21±2°C and a humidity of approximately 40 %. The specimens were loaded by constant force amplitude P_a.

Theoretical background

Two models were used to analyze fatigue data; the first model that was applied to broken specimens from fatigue tests was the Basquin's model [20]. It is a basic model describing fatigue. It is given by a simple equation that indicates the dependence of stress amplitude on the number of cycles after failure (See Eqn. 1).

$$\Delta\sigma(N) = aN^b \tag{1}$$

In addition to the deterministic Basquin model, a probabilistic evaluation using the Castillo–Canteli model was performed in order to account for statistical scatter in fatigue life [19]. The model is based on the compatibility between probability distributions describing the variance in terms of lifetime and load conditions. i.e. $F(N;\Delta\sigma)$ and $F(\Delta\sigma;N)$. The Weibull distribution was used in this analysis, this includes the parameters of location (λ), scale (δ) and shape (β). The model is given by Eqn. 2:

$$Pf\left(N.\Delta\sigma\right) = 1 - exp\left\{-\left[\frac{\left(logN - B\right)\left(log\Delta\sigma - C\right) - \lambda}{\delta}\right]^{\beta}\right\} \tag{2}$$

Figure 6. Experimental set up for fatigue: ZwickRoell Vibrophore resonance pulsator with specimens.

RESULTS

Results of corrosion

The amount of corrosion on the specimens was meticulously measured and quantified to provide a clear understanding of the extent of damage sustained under various exposure conditions. Quantifying corrosion is critical for understanding its effect on fatigue performance. Quantifying corrosion damage is essential for evaluating its influence on fatigue performance.

The mass loss due to corrosion was determined for each specimen before and after exposure. The findings, which include corrosion loss in grams and grams per square meter, are presented in the following sections and tables. This thorough quantification yields a clear indication of corrosion damage for each exposure condition.

The uncorroded specimens exhibited a bright metallic surface (Fig. 5). With increasing corrosion exposure, the metallic luster gradually disappeared, and corrosion products formed on the specimen surface. Localized corrosion pits became more pronounced with increasing exposure time (3 days, 6 days, and 6 + 3 days), which act as stress concentrators and promote fatigue crack initiation.

After completing the rust removal process, a visual inspection reveals a hierarchical distribution of corrosion pits, with varying degrees of damage in each area. This observation indicates that as the corrosion duration increases (3 (35°C), 6 (35°C) and 6 (35°C) +3 (50°C) days), the size of corrosion pits gradually grows.

To investigate the evolutionary pattern of time-varying corrosion damage in S460NL, the remaining weight of specimens was measured at different corrosion durations. The measured data revealed a certain deviation between the weights of corroded specimens in 3 (35°C), 6 (35°C) and 6 (35°C) + 3 (50°C) days and those without corrosion. Therefore, this study introduces several parameters for analysis, namely the measured corrosion loss, standard deviation s and coefficient of variation c. According to the data presented in Tab. 3, the mass loss rate of the specimens increases with increasing corrosion exposure time.

- Note: Specimen dimension - d = 4 mm. l = 24 mm. A = 302 mm² = 0.000302 m².

Time of exposition days (temperature)	n	Before test (g)	After test (g)	Corrosion loss (g)	Mean corrosion loss (g)	s (g)	Corrosion loss (g/m²)	Mean corrosion loss (g/m²)	s (g/m2)	c (-)
	1	2.116	2.092	0.024			79.577			
	2	2.263	2.239	0.024			79.577			
3 (35°C)	3	2.267	2.238	0.029	0.028	0.00413	96.156	94.167	13.687	0.145
	4	2.283	2.248	0.035			116.050			
	5	2.248	2.218	0.030			99.472			
	1	2.063	2.030	0.033			109.419			
	2	2.086	2.039	0.047			155.839			
6 (35°C)	3	2.236	2.186	0.050	0.041	0.00634	165.786	136.608	21.012	0.154
	4	2.248	2.209	0.039			129.313			
	5	2.176	2.139	0.037			122.682			
	1	2.270	2.189	0.081			268.574			
	2	2.261	2.182	0.079			261.943			
6 (35°C) + 3 (50°C)	3	2.267	2.200	0.067	0.072	0.00958	222.154	237.406	31.776	0.134
	4	2.237	2.182	0.055			182.365			
	5	2.330	2.254	0.076			251.995			

Table 3. Test results of corrosion parameters under different corrosion times.

Results of fatigue test

The relationship between the stress amplitude (σ_a) and the number of cycles to failure (N) for S460NL steel under different corrosion conditions is represented by the S-N curves. Fig. 7 illustrates how fatigue resistance clearly declines as exposure to corrosive environments increases.

The specimens exposed to combined 6 (35°C) + 3 (50°C) days of corrosion show the greatest reduction in fatigue life, whereas the reference specimens, which were not subjected to any corrosion, show the highest fatigue resistance. The Basquin's model parameters (a, b) with the coefficients of determination (R^2) and endurance limit σ_c (1×10^7) for studied different conditions are summarized in Tab. 4.

- **Reference Specimens**: The reference specimens exhibit a relatively shallow slope b and the lowest value of parameter a. indicating a higher fatigue strength. The data appear to have moderate variability, though, based on the R^2 value of 0.82 and endurance limit is the highest value 214 MPa.
- **Corroded for 3 (35°C) Days**: This condition has a steeper slope b and a significant increase in parameter a. Its R^2 value of 0.87 indicating a good model fit and a notable decrease in fatigue resistance with endurance limit of 176 MPa.
- **Corroded for 6 (35°C) Days**: With an R^2 of 0.97, the parameters a and b show a further decline in fatigue resistance in comparison to the 3-day corrosion and decrease in endurance limit to 135 MPa.
- **Corroded for 6 (35°C) + 3 (50°C) Days**: With the highest values of a and b and an excellent fit with a R^2 of 0.96, this condition exhibits the most severe reduction in fatigue resistance corresponding to an endurance limit of 92 MPa.
- **Corroded on the Exterior**: Specimens subjected to natural corrosion show intermediate a and b values with a high R^2 of 0.97, suggesting a notable albeit milder reduction in comparison to the for 6 (35°C) + 3 (50°C) days condition.

Condition	a	b	R^2	σ_c (1×10^7) [MPa]
Reference specimens	342.75	-0.029	0.82	214
Corroded for 3 (35°C) days	357.48	-0.044	0.87	176
Corroded for 6 (35°C) days	468.93	-0.077	0.97	135
Corroded for 6 (35°C) + 3 (50°C) days	756.72	-0.131	0.96	92
Corroded on the exterior	418.37	-0.052	0.97	181

Table 4. Basquin's parameters and determination coefficients.

If we compare the fatigue behavior, shown graphically in Fig. 7. We can see a clear pattern of a downward trend in fatigue resistance depending on the length of time the specimens are exposed to the corrosive environment. Some specimens did not fail within the maximum test duration of 10^7 cycles and were therefore classified as run-outs. These tests were stopped at the predefined cycle limit and treated as right-censored data in the statistical fatigue analysis performed using the Castillo–Canteli Weibull model.

The parameters of the probabilistic Castillo–Canteli Weibull fatigue model (B, C, β, δ, λ and σ∞) for the different corrosion conditions are summarized in Tab. 5. The parameter σ∞ represents the asymptotic stress parameter of the probabilistic model and should not be interpreted directly as the engineering endurance limit.

- **Reference Specimens**: The fitted model yields $\sigma\infty$ = 214 MPa, indicating the highest fatigue resistance among all investigated conditions. The parameters B, C, β, δ and λ describe the probabilistic S–N field with moderate variability.
- **Corroded for 3 (35°C) days**: The $\sigma\infty$ parameter decreases to 176 MPa, reflecting the reduction in fatigue resistance caused by the initial corrosion damage. The relatively high β value indicates increased variability of fatigue life.
- **Corroded for 6 (35°C) days**: The model parameters indicate a further reduction in fatigue resistance, with σ∞ decreasing to 123 MPa compared with the 3-day corrosion condition.
- **Corroded for 6 (35°C) + 3 (50°C) days**: The fitted model yields the lowest σ∞ value (28.8 MPa), reflecting the severe degradation of fatigue resistance. It should be noted that σ∞ is a parameter of the probabilistic Castillo–

Canteli model and does not correspond directly to the engineering endurance limit obtained from the Basquin model.

- **Corroded on the Exterior**: The fitted σ∞ value of 179 MPa indicates an intermediate level of fatigue degradation compared with the artificially corroded specimens.

Condition	B	C	β	δ	λ	$\sigma\infty$ (Castillo–Canteli parameter) [MPa]
Reference specimens	10.35	5.37	2.45	0.20	0.00	214
Corroded for 3 (35°C) days	9.63	5.17	7.34	0.16	0.12	176
Corroded for 6 (35°C) days	7.48	4.82	2.01	0.49	1.14	123
Corroded for 6 (35°C) + 3 (50°C) days	0	3.36	4.94	4.83	15.31	29
Corroded on the exterior	10.09	5.19	3.48	0.37	0.04	179

Table 5. Castillo-Canteli model parameters and determination coefficients.

The probabilistic Castillo–Canteli model allows the statistical scatter of fatigue life to be captured and provides a more realistic representation of fatigue behavior compared to deterministic approaches.

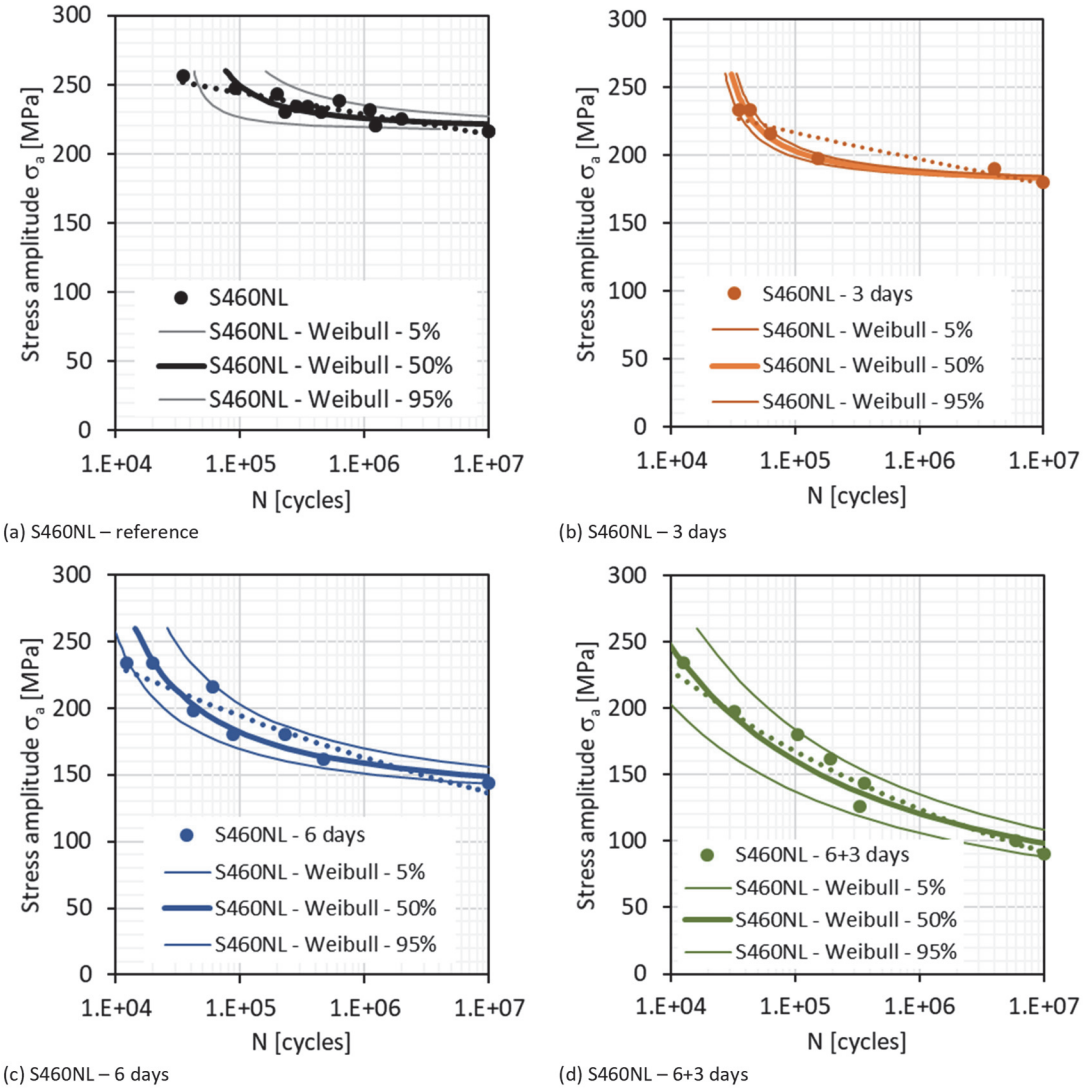

(a) S460NL – reference (b) S460NL – 3 days

(c) S460NL – 6 days (d) S460NL – 6+3 days

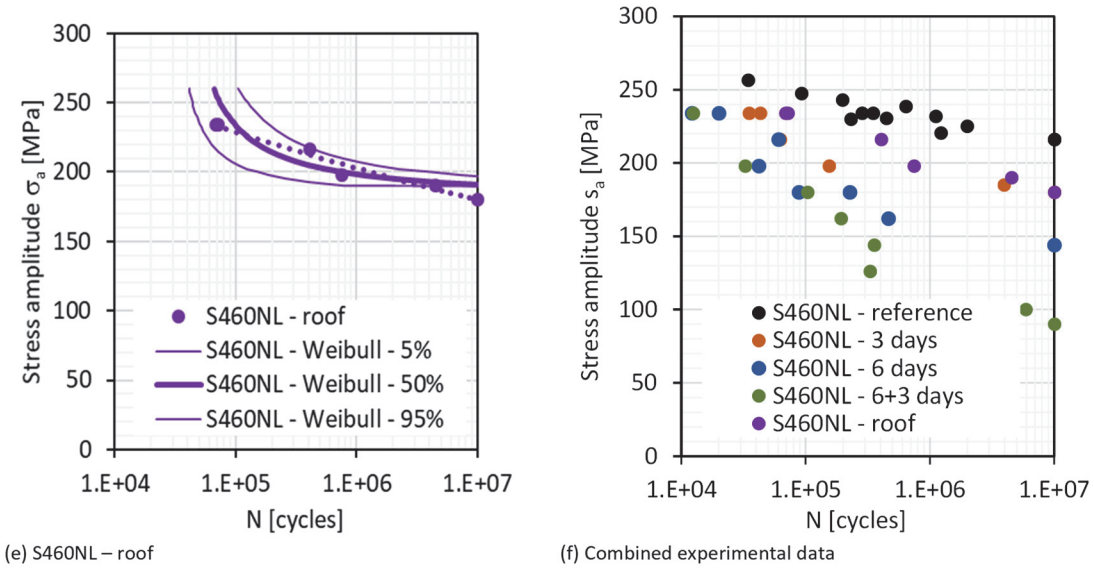

(e) S460NL – roof (f) Combined experimental data

Figure 7: S–N curves of S460NL steel under different corrosion conditions: (a–e) Experimental fatigue data with Weibull statistical fits (5%, 50%, and 95%) obtained using the Castillo–Canteli model. (f) Combined diagram showing all experimental fatigue failure data points for direct comparison between corrosion exposure conditions.

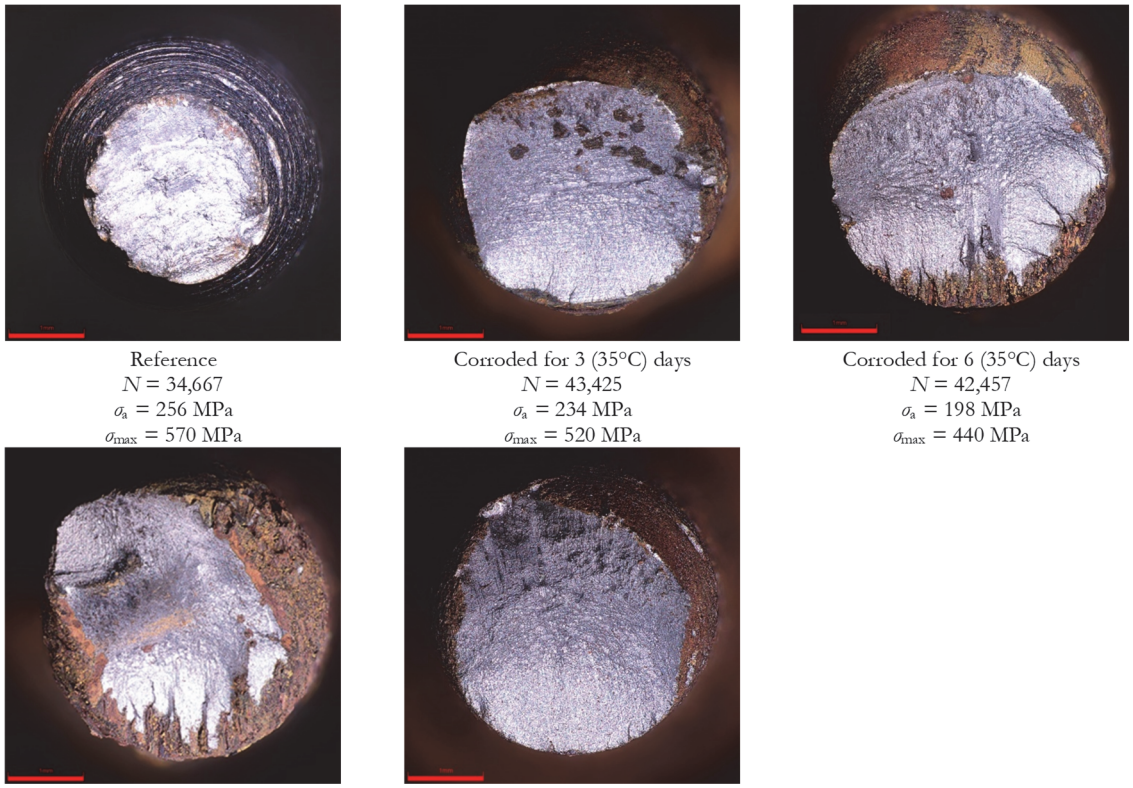

Reference
N = 34,667
σ_a = 256 MPa
σ_{max} = 570 MPa

Corroded for 3 (35°C) days
N = 43,425
σ_a = 234 MPa
σ_{max} = 520 MPa

Corroded for 6 (35°C) days
N = 42,457
σ_a = 198 MPa
σ_{max} = 440 MPa

Corroded for 6 (35°C) + 3 (50°C) days
N = 32,583
σ_a = 198 MPa
σ_{max} = 440 MPa

Corroded on the exterior
N = 72,263
σ_a = 234 MPa
σ_{max} = 520 MPa

Figure 8. A set of photographs of fracture surfaces of steel specimens for the region of approximately 40,000 cycles.

Fatigue fracture analysis

Photographs of fracture surfaces of broken specimens were taken on an Olympus DXS 1000 digital microscope.

Three fatigue life regions were selected for fracture surface analysis. The first area that was monitored was around 40,000 cycles. The photo always comes from a specimen that was as close as possible to this number of cycles. We can notice that in the specimens that were significantly burdened by corrosion, there are intrusions, which subsequently lead to cracks (Fig. 8). These further weaken the cross-section of the stressed specimen until brittle fracture occurs.
In the second observed area around 200,000 cycles, we can observe that the intrusions are no longer significant (Fig. 9). The place of initiation and the area of accelerated fracture development up to the fracture zone can be better determined

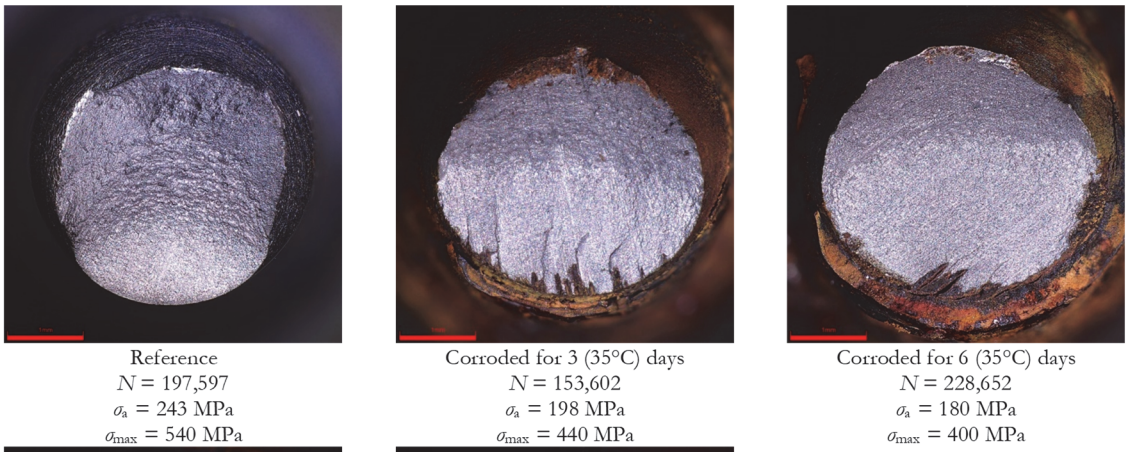

Reference
N = 197,597
σ_a = 243 MPa
σ_{max} = 540 MPa

Corroded for 3 (35°C) days
N = 153,602
σ_a = 198 MPa
σ_{max} = 440 MPa

Corroded for 6 (35°C) days
N = 228,652
σ_a = 180 MPa
σ_{max} = 400 MPa

Corroded for 6 (35°C) + 3 (50°C) days
N = 193,457
σ_a = 162 MPa
σ_{max} = 360 MPa

Corroded on the exterior
N = 408,255
σ_a = 216 MPa
σ_{max} = 480 MPa

Figure 9. A set of photographs of fracture surfaces of steel specimens for the region of approximately 200,000 cycles.

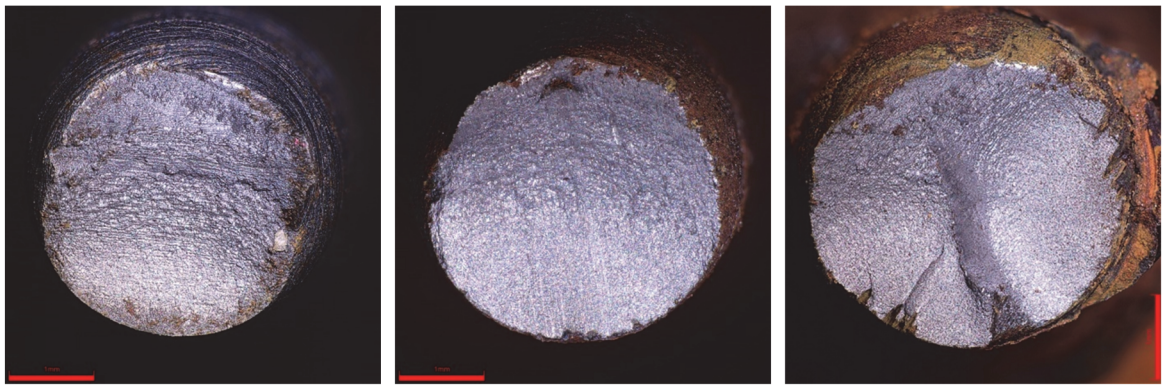

Reference
N = 636,904
σ_a = 239 MPa
σ_{max} = 530 MPa

Corroded on the exterior
N = 748,953
σ_a = 198 MPa
σ_{max} = 440 MPa

Corroded for 6 (35°C) + 3 (50°C) days
N = 464,266
σ_a = 162 MPa
σ_{max} = 360 MPa

Figure 10. A set of photographs of fracture surfaces of steel specimens for the region of approximately 600,000 cycles.

For the last observed area around 600,000, it was no longer possible to test specimens from all sets (Fig. 10). From the photos of the 3 specimens, we can see similar behavior to the previous area. Intrusions continue to decrease.
These results confirm that increasing corrosion severity leads to a progressive reduction in fatigue resistance. The observed trend indicates that corrosion-induced surface damage acts as a dominant factor governing fatigue crack initiation and significantly shortens fatigue life under cyclic loading.

Discussion

The comparison of S–N curves for S460NL steel under different corrosion conditions is presented in Fig. 11, where selected cycle levels (40,000; 200,000; and 600,000 cycles) are indicated by vertical dashed lines. These cycle levels were selected for the purpose of monitoring the evolution of fracture surfaces during fatigue loading. The delineated regions correspond to areas where fracture surface observations were conducted. Fractographic analysis using an Olympus DSX1000 digital microscope revealed that specimens exposed to corrosion exhibited crack initiation at or near the outer surface. Conversely, the reference specimens predominantly exhibited crack initiation at surface imperfections that were not associated with corrosion. The presence of corrosion pits has been shown to significantly increase local stress concentration, thereby promoting earlier crack initiation and, consequently, reducing fatigue life.
The fracture surfaces of the corroded specimens are exhibited in Fig. 8, Fig. 9, and Fig. 10. The fracture morphology reveals a region of smoothness in proximity to the site of crack initiation, succeeded by the presence of visible fatigue striations, which are indicative of crack propagation toward the final fracture zone. The final fracture region exhibits characteristics indicative of cleavage fracture, suggesting a predominantly brittle failure mechanism in the final stage of crack growth.
The experimentally obtained *S–N* curves demonstrate a clear reduction in fatigue life with increasing corrosion severity. Specimens exposed to corrosion for 3 days, 6 days, and 6+3 days, as well as those exposed to natural atmospheric corrosion on the roof, all exhibit shorter fatigue lives compared with the reference specimens. The reduction becomes more pronounced in the high-cycle fatigue region, where fatigue performance is highly sensitive to surface conditions.
This behavior can be attributed primarily to the formation of corrosion pits, which act as stress concentrators. Pitting corrosion, once it has occurred, causes a substantial deterioration of the surface integrity of S460NL steel, thereby facilitating fatigue crack initiation. The presence of larger and deeper corrosion pits has been shown to produce higher stress concentration factors, which have been demonstrated to accelerate crack initiation and reduce the fatigue life of the material.

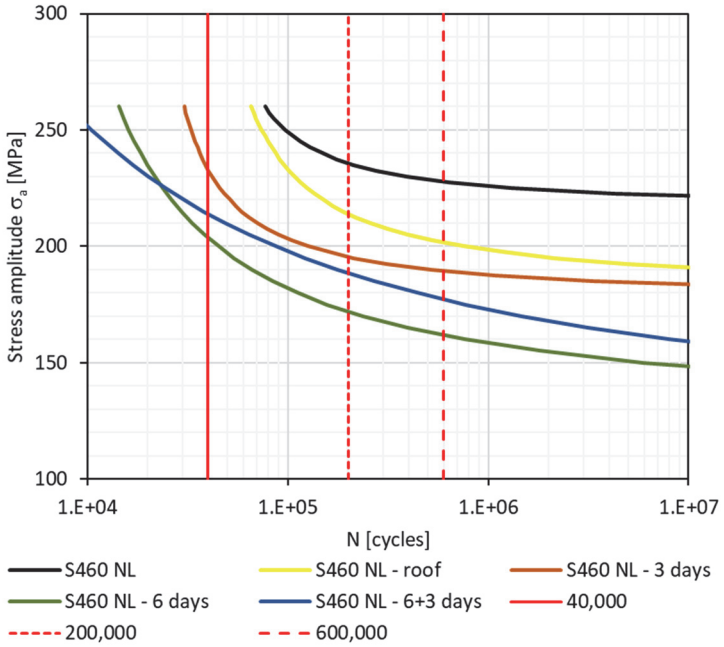

Figure 11. Comparison of S460NL *S-N* curves with different corrosion with marked areas/numbers for monitoring of fracture surfaces.

Condition	σ_a [MPa] N =100,000	Reduction [%] $\left(1-\sigma_{acr} / \sigma_{aref}\right)*100$	σ_c [MPa] N_c = 10,000,000	Reduction [%] $\left(1-\sigma_{acr} / \sigma_{aref}\right)*100$
Reference specimens	247	-	214	-
Corroded for 3 (35°C) days	204	17.5	176	17.7
Corroded for 6 (35°C) days	182	26.4	135	36.9
Corroded for 6 (35°C) + 3 (50°C) days	164	33.8	92	57.0

Table 6. Fatigue Resistance Reduction.

The quantitative reduction in fatigue resistance for the investigated corrosion conditions is summarized in Tab. 6. The results indicate:

- Corroded for 3 days: reduction of approximately 17.7% at 10^7 cycles and 17.5% at 10^5 cycles.
- Corroded for 6 days: reduction of 26.4% at 10^5 cycles and 36.9% at 10^7 cycles.
- Corroded for 6+3 days: the most severe degradation with 33.8% reduction at 10^5 cycles and 57.0% reduction at 10^7 cycles.

These results confirm that fatigue degradation increases significantly with corrosion exposure time.
The relationship between corrosion damage and fatigue resistance is further illustrated in Fig. 12, which shows the correlation between corrosion mass loss and normalized endurance limit derived from the Basquin model. The endurance limit of corroded specimens is normalized by the corresponding endurance limit of the uncorroded reference specimens.

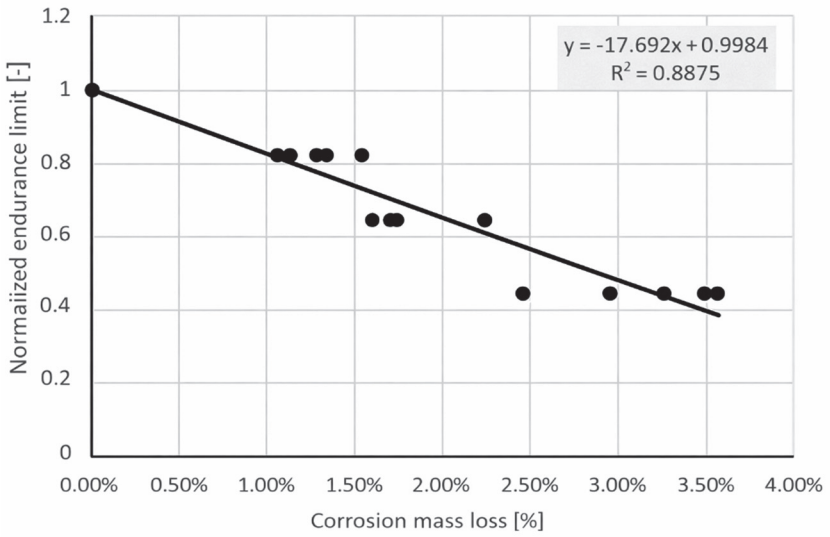

Figure 12. Relationship between corrosion mass loss and normalized endurance limit of S460NL steel derived from Basquin's law.

As shown in Fig. 12, the normalized endurance limit decreases approximately linearly with increasing corrosion mass loss. This trend demonstrates that corrosion-induced surface damage plays a dominant role in reducing the fatigue resistance of S460NL steel.

Conclusion

This study investigated the influence of corrosion damage on the fatigue behavior of S460NL high-strength steel using experimental fatigue testing combined with statistical modeling.
The findings indicate that corrosion exerts a substantial deleterious effect on fatigue resistance. The reference specimens demonstrated the highest fatigue performance, while specimens subjected to accelerated corrosion environments exhibited a progressive decline in fatigue life.

Specimens exposed to combined corrosion for 6 (35°C) + 3 (50°C) days exhibited the most severe degradation in fatigue behavior. In this condition, the endurance limit decreased to approximately 92 MPa, representing a reduction of nearly 57% compared with the reference material. It has been demonstrated that specimens exposed to natural atmospheric corrosion on the roof exhibited fatigue behavior that was comparable to specimens exposed to laboratory corrosion for 3–6 days. This finding indicates that real environmental exposure can produce a measurable reduction in fatigue resistance, even over relatively short periods.

The experimental *S–N* curves were successfully described using both the Basquin model and the probabilistic Castillo–Canteli model, which showed good agreement with the measured fatigue data for most corrosion conditions.

Overall, the results demonstrate that corrosion-induced surface damage substantially diminishes the fatigue resistance of S460NL steel, with the extent of degradation escalating in proportion to the duration of corrosion exposure. These findings underscore the necessity of incorporating corrosion effects into the assessment of the fatigue life of steel structures and underscore the importance of implementing effective corrosion protection strategies in structural applications.

In addition to corrosion mass loss, surface roughness has been demonstrated to play a significant role in the fatigue degradation of corroded materials. The formation of corrosion pits and surface irregularities has been shown to increase local stress concentration and promote earlier fatigue crack initiation. Although surface roughness measurements were not included in the present study's scope, future investigations could incorporate quantitative roughness characterization and evaluate its correlation with fatigue resistance. Such an approach has the potential to enhance the practical applicability of corrosion–fatigue assessment for structural steel components.

Acknowledgments

Financial support from specific research of Brno University of Technology No. FAST-S-25-8839 – Comprehensive Investigation and Quantification of Fatigue Behavior in High-Strength Structural Steel Under Varied Conditions. The 3rd authors would like to acknowledge to the project No. CZ.02.01.01/00/22_008/0004631. Materials and technologies for sustainable development within the Jan Amos Komensky Operational Program financed by the European Union and from the state budget of the Czech Republic.

Data Availability

The data used in this study is available at: DOI: https://doi.org/10.5281/zenodo.13329896

References

[1] European Committee for Standardization. EN 1993-1-1: Eurocode 3: Design of steel structures - Part 1-1: General rules and rules for buildings (1993), 3.

[2] European Committee for Standardization. Eurocode 3 - Design of steel structures - Part 1-12: Additional rules for the extension of EN 1993 up to steel grades S 700 (2007).

[3] Viaduc de Millau. Compagnie Eiffage du. A structure, a heritage (2004). https://www.leviaducdemillau.com.

[4] ØRESUNDSBRON. A structure, a heritage. Viaduc de Millau (2000). https://www.oresundsbron.com/.

[5] Climie, D., Shackman, L. (2019). Construction of the Queensferry Crossing and approach roads in Scotland (part 2). Proceedings of the Institution of Civil Engineers - Civil Engineering 172, pp. 121–129. DOI: https://doi.org/10.1680/jcien.18.00047.

[6] Xue, S. (2025). Fatigue failure analysis of high-strength steel in seawater corrosion environment. Npj Materials Degradation, 9(1), 153. DOI: https://doi.org/10.1038/s41529-025-00703-6.

[7] Dong, L., Wu, M., Ling, D., Wang, H., Zheng, H., Ma, C., (2025). Simultaneously improving corrosion and fatigue resistance of A100 steel by laser assisted ultrasonic nanocrystal surface modification. Int J Fatigue 199, 109056. DOI: https://doi.org/10.1016/j.corsci.2025.112749.

[8] Yao, J., Zhong, X., Zhang, Z., Fan, Z., Hu, J., Wang, J. (2024). The fitness and corrosion mechanisms of high-strength steel in corrosive oil–water environment at high temperature. Materials and Corrosion, 75, pp. 247–265.

DOI: https://doi.org/10.1002/MACO.202313912.
[9] Malíková, L., Benešová, A., Al Khazali, M., Seitl, S. (2024). Corrosion vs. fatigue in a high-strength steel specimen investigated via FEM. Procedia Structural Integrity, 58, pp. 73–79. DOI : https://doi.org/10.1016/J.PROSTR.2024.05.012.
[10] Avramenko, T., Michel, S., Stutz, A., Kollender, J., Burda, I., Hans, U. (2025). A Comparative Study on Corrosion Fatigue Susceptibility and Microstructural Effects in 6061-T6 and 6082-T6 Aluminum Alloys. Metals 15, 653. DOI: https://doi.org/10.3390/met15060653.
[11] Hejazi, B., Compart, A., Fritsch, T., Wagner, R., Weidner, A., Biermann, H. (2025). Fatigue Crack Segmentation and Characterization of Additively Manufactured Ti-6Al-4V Using X-Ray Computed Tomography. Fatigue Fract Eng Mater Struct, 48, pp. 204–216. DOI: https://doi.org/10.1111/FFE.14489.
[12] Zhang, Y., Hu, L., Shen, C., Zhao, X.L. (2024). Study on fatigue behavior of butt-welded high-strength steel connections with surface cracks. Thin-Walled Structures, 200, 111888. DOI:https://doi.org/10.1016/J.TWS.2024.111888.
[13] Malíková, L., Miarka, P. (2024). Fatigue crack propagation near a corrosion pit in a HSS specimen. Theoretical and Applied Fracture Mechanics, 129, 104214. DOI: https://doi.org/10.1016/J.TAFMEC.2023.104214.
[14] Liu, X., Yan, B., Sun, H. (2023). Fatigue Life Prediction of High Strength Steel with Pitting Corrosion under Three-Point Bending Load. Metals, 13, 1839. DOI: https://doi.org/10.3390/met13111839.
[15] Fan, W., Zhou, Y., Cheng, P., Peng, W. (2024). Study on fatigue properties and life prediction of corroded steel strands. J Constr Steel Res, 217, 108636. DOI: https://doi.org/10.1016/j.jcsr.2024.108636.
[16] Jie, Z., Zhang, Z., Susmel, L., Zhang, L., Lu, W. (2024). Corrosion fatigue mechanisms and evaluation methods of high-strength steel wires: A state-of-the-art review. Fatigue Fract Eng Mater Struct, 47, pp. 2287–2318. DOI: https://doi.org/10.1111/ffe.14311.
[17] Krejsa, M., Brozovsky, J., Lehner, P., Parenica, P., Seitl, S., Krejsa, M., (2025). Fatigue resistance of structural elements made from high-strength steel. AIPC, 3315, 120003. DOI: https://doi.org/10.1063/5.0286010.
[18] Alcántara, J., de la Fuente, D., Chico, B., Simancas, J., Díaz, I., Morcillo, M. (2017). Marine Atmospheric Corrosion of Carbon Steel: A Review. Materials, 10. DOI: https://doi.org/10.3390/MA10040406.
[19] Fernández Canteli, A., Castillo, E., Blasón, S., Correia, J.A.F.O., de Jesus, A.M.P. (2022). Generalization of the Weibull probabilistic compatible model to assess fatigue data into three domains: LCF, HCF and VHCF. Int J Fatigue, 159, 106771. DOI: https://doi.org/10.1016/j.ijfatigue.2022.106771.
[20] Seitl, S., Miarka, P., Klusák, J., Kala, Z., Krejsa, M., Blasón, S. (2018). Evaluation of fatigue properties of S355 J0 steel using ProFatigue and ProPagation software. Procedia Structural Integrity, 13, pp. 1494–1501. DOI: https://doi.org/10.1016/J.PROSTR.2018.12.307.
[21] British Standards Institution (BSI). BS EN 10025-6:2004+A1:2009 - Hot rolled products of structural steels - Part 6: Technical delivery conditions for flat products of high yields strength structural steels in the quenched and tempered condition 2004.
[22] ASTM. E466 Standard Practice for Conducting Force Controlled Constant Amplitude Axial Fatigue Tests of Metallic Materials (2021). https://doi.org/10.1520/E0466-21.
[23] International Organization for Standardization (ISO). ISO 9227, (2022) - Corrosion tests in artificial atmospheres — Salt spray tests. https://www.iso.org/standard/81744.html.